Mapping the Distribution of the Outer Hair Cell Motility Voltage Sensor by Electrical Amputation

Guojie Huang and J. Santos-Sacchi
Sections of Otolaryngology and Neurobiology, Yale University School of Medicine, New Haven, Connecticut 06510 USA

ABSTRACT The outer hair cell (OHC) possesses a nonlinear charge movement whose characteristics indicate that it represents the voltage sensor responsible for OHC mechanical activity. OHC mechanical activity is known to exist along a restricted extent of the cell's length. We have used a simultaneous partitioning microchamber and whole cell voltage clamp technique to electrically isolate sections of the OHC membrane and find that the nonlinear charge movement is also restricted along the cell's length. Apical and basal portions of the OHC are devoid of voltage sensors, corresponding to regions of the cell where the subsurface cisternae and/or the mechanical responses are absent. We conclude that the physical domain of the motility voltage sensor corresponds to that of the mechanical effector and speculate that sensor and effector reside within one intra membranous molecular species, perhaps an evolved nonconducting or poorly conducting voltage-dependent ion channel.

INTRODUCTION

The peripheral auditory system is responsible for the initial decoding of spectral information within acoustic stimuli. In the mammal, frequency selectivity and sensitivity afforded by Bekesy's basilar membrane traveling wave is enhanced by a metabolically labile process which involves one of the two types of sensory cells which populate the organ of Corti, the outer hair cells (OHC). Following the discovery of electrically induced OHC motility (Brownell et al., 1985), evidence has accumulated that the mechanical activity of the OHC alters basilar membrane motion in such a way as to enhance the tuning characteristics of inner hair cells and eight nerve fibers (Ruggero, 1992).

OHC motility is transmembrane voltage-dependent (Santos-Sacchi and Dilger, 1988; Iwasa and Kachar, 1989). Hyperpolarization elongates and depolarization shortens the cylindrically shaped cell. The mechanism underlying this shape change which can occur at acoustic frequencies is unknown. However, it is not based on typical cellular mechanisms of motility (Kachar et al., 1986; Santos-Sacchi and Dilger, 1988; Holley and Ashmore, 1988). In fact, recent evidence indicates that the force generating mechanism may reside within the plasma membrane itself, possibly corresponding to 8–10-nm intramembranous particles observed ultrastructurally in the lateral plasmalemma (Kalinec et al., 1992).

Nonlinear charge movement in the OHC, which is believed to be indicative of a motility voltage sensor, has been studied (Ashmore, 1989, 1992; Santos-Sacchi, 1990, 1991a, 1992), and many characteristics of the mechanical response and charge movement coincide. Recently, Dallos et al. (1991) have utilized a partitioning microchamber to map the distribution of the mechanical response along the length of the cylindrical OHC, and found that it resides within a central region, roughly corresponding to the extent of the subsurface cisternae, an intracellular membranous system lying beneath the plasma membrane. Ashmore (1992) presented preliminary evidence that the nonlinear charge movement measured in cell-attached patches exists on the lateral portion of the cell, but is absent on the basal end. We have evaluated the extent of the motility voltage sensor using a combined microchamber and whole cell voltage clamp technique which enables us to electrically amputate portions of the OHC. We conclude that the distribution of the motility voltage sensor corresponds to the extent of the mechanical responses observed with the partitioning microchamber (Dallos et al., 1991), that is, that sensor and effector mechanisms colocalize.

A preliminary account of this work has been presented (Santos-Sacchi and Huang, 1993).

MATERIALS AND METHODS

General

Guinea pigs were overdosed with halothane. The temporal bones were removed, the apical two turns of the organ of Corti were microdissected free, and OHCs were isolated enzymatically with collagenase (0.3 mg/ml for 10 min followed by gentle reflux through a tapered polyethylene pipette tip) in Medium 199 with Hanks' salts (GIBCO). The cell-enriched supernatant was then transferred to a 700-μl perfusion chamber, and the cells were permitted to settle onto the cover glass bottom. All experiments were performed at room temperature (~23°C). A Nikon Diaphot inverted microscope with Hoffmann optics was used to observe the cells during electrical recording. Experiments were videotaped. A modified Leibovitz medium (100 mM NaCl, 5.37 mM KCl, 2.0 mM $CoCl_2$, 1.48 mM $MgCl_2$, 20 mM tetra ethyl ammonium, 2 μM tetrodotoxin, 20 mM CsCl, 5.0 mM 4-(2-hydroxyethyl)-1-piperazineethanesulfonic acid, 5.0 mM dextrose, pH 7.2) was used in order to block ionic conductances (outward and inward K^+, Ca^{2+}, Na^+) which might otherwise interfere with capacitive current measures. OHCs maintained normal appearance in this solution for up to an hour. Osmolarity was adjusted to 300 mOsm with dextrose.

Electrical Recording

OHCs were whole cell voltage-clamped with a Dagan 8900 patch clamp amplifier at a holding potential of −80 mV, similar to the potential recorded

Received for publication 26 April 1993 and in final form 26 July 1993.
Address reprint requests to Joseph Santos-Sacchi, PhD.

0006-3495/93/11/2228/09 $2.00

in vivo (Dallos et al., 1982). Pipette solutions were composed of 140 mM CsCl, 10 mM EGTA, 5 mM tetra ethyl ammonium, 2 mM $MgCl_2$, and 5 mM 4-(2-hydroxyethyl)-1-piperazineethanesulfonic acid buffered to pH 7.2. Osmolarity was adjusted to 300 mOsm with dextrose. Gigohm seals were obtained either at the nuclear level of the cell membrane or just beneath the cuticular plate depending upon experimental intent; electrode capacitance and series resistance were compensated prior to whole cell recording. A modified version of Clampex (Axon Instruments, CA) utilizing the Labmaster board was used to collect data which were saved to disk for off-line analysis. Current was filtered at 5 kHz with an eight-pole Bessel filter.

Determination of nonlinear capacitance

The electrical characteristics of the voltage-clamped OHC when ionic conductances are blocked can be modeled most simply as an electrode resistance (access resistance, R_s) in series with a parallel combination of a membrane resistance (R_m), a linear membrane capacitance (C_{lin}), and a voltage-dependent membrane capacitance (C_v) (Fig. 1 *A*). The total membrane capacitance (C_m) at any given voltage is the sum of the linear and nonlinear capacitances,

$$C_m = C_v + C_{lin}, \tag{1}$$

where C_v, which results from the nonlinear charge movement associated with the motility voltage sensor, is defined as the first derivative of the two-state Boltzmann function ($Q_v = Q_{max}/(1 + \exp(-ze(V_m - V_h)/kT))$ which has been shown to adequately relate OHC nonlinear charge movement and membrane voltage ($C_v = dQ_v/dV_m$; see Santos-Sacchi (1991a)). Thus,

$$C_v = \frac{\left(Q_{max}\frac{ze}{kT}\right)}{\exp\left(\frac{ze}{kT}\{V_m - V_h\}\right)\left[1 + \exp\left(\frac{-ze}{kT}\{V_m - V_h\}\right)\right]^2}, \tag{2}$$

where V_m is the membrane potential, V_h is voltage at half-maximal nonlinear charge transfer, e is electron charge, k is Boltzmann's constant, T is absolute temperature, z is the valence, and Q_{max} is maximum nonlinear charge transfer. Fits of the measured capacitance data with this equation permit the estimation of nonlinear charge characteristics, similar to measures of these characteristics determined by subtraction techniques (e.g., *P*/−4) which have been utilized previously (Santos-Sacchi, 1991a).

The method employed to estimate membrane capacitance (C_m) and series resistance (R_s) is based on a linearized circuit at small excitation voltage steps (V_c). It is robust despite filter settings and accurately takes into account the effects of series resistance on capacitance measures (Santos-Sacchi, 1993).

For each response at a given step voltage (Fig. 1, *b* and *c*; see Appendix),

$$C_m = \left(\frac{R_{in}}{R_m}\right)^2\frac{Q}{V_c} \tag{3}$$

$$R_s = \frac{R_{in}\tau V_c}{QR_{in} + \tau V_c}, \tag{4}$$

where

$$R_{in} = R_m + R_s, \tag{5}$$

the input resistance readily obtained at steady state. V_c is the raw command voltage. The time constant (τ) is a single exponential fit to the decaying capacitive current induced by the voltage step, and the charge (Q) is obtained by integration (Fig. 1 *D*). Eq. 3 had been identified and used by Mathias et al. (1981) to evaluate alternative explanations of nonlinear gating charge movement. It is the proper evaluation of cell capacitance for the cell model when the ratio of R_s and R_m does not approach zero. In this report, voltage and charge were corrected for residual series resistance effects. Furthermore, to account for voltage step size, the voltages used in the fits of the capacitance data to Eq. 1 were taken to be the corrected voltage prior to the step plus one-half the corrected step voltage, i.e., the average voltage,

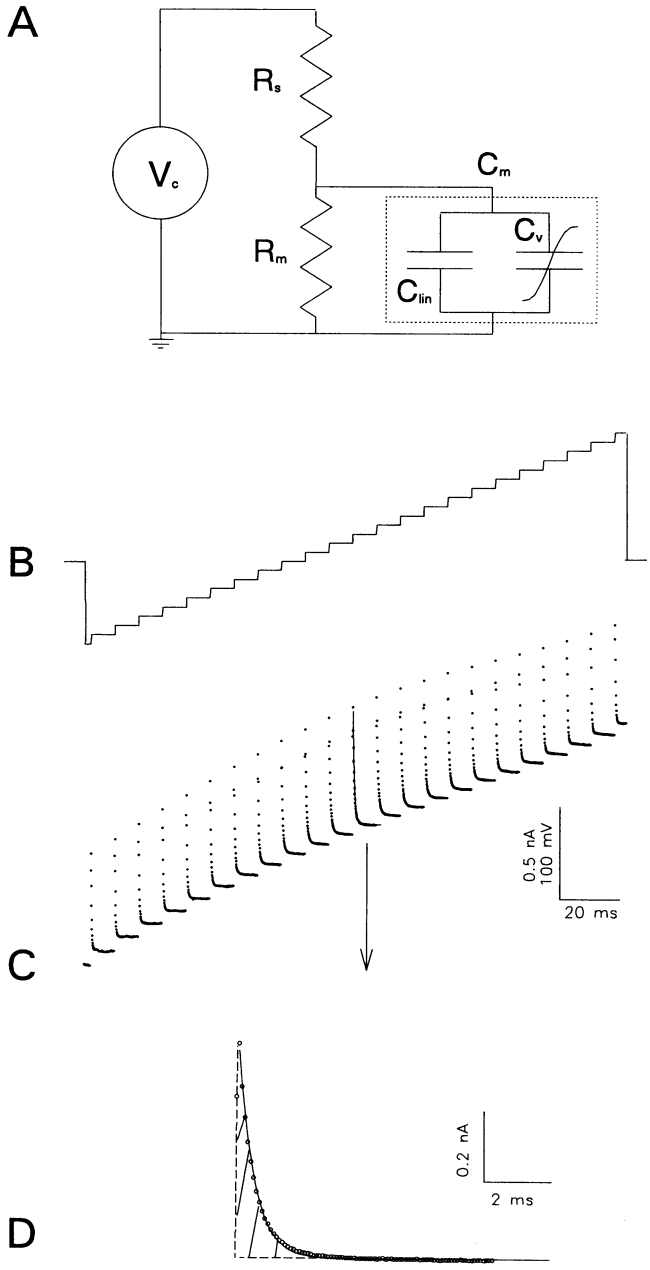

FIGURE 1 (*A*) Schematic of the OHC under voltage clamp. R_s, series resistance; R_m membrane resistance; C_m, membrane capacitance composed of the parallel combination of a voltage-dependent capacitance (C_v) and linear capacitance (C_{lin}). (*B*) Voltage stair protocol. Holding potential was −80 mV. (*C*) Typical current record obtained from an OHC. For illustration, only one transient response is fitted to the extent of ten times its time constant. (*D*) Data and single exponential fit from above with expanded time scale. Charge was determined by integration of the shaded region.

as is predicted through modeling. All data analysis was performed with the software package MATLAB (Mathworks, Natick, MA). Fits of the data to Eq. 1 were made with the Nelder-Mead simplex algorithm.

The voltage protocol was a stair stimulus (2048 pts) whose nominal step size was 10 mV (Fig. 1 *B*), and whose step length was automatically adjusted to 10 times the previously determined time constant at the holding potential of −80 mV. Current records are averages of 20 collections. Since the time constant at each step potential is influenced by the OHC's nonlinear capacitance and any residual nonlinear leakage conductance, it was impossible

to guarantee that the decaying current trace would reach steady state for each step potential (Fig. 1 *C*). In order to overcome this limitation, the length of the exponential fit was extended to 10 times the fitted time constant and the fit was used for Q determination. The exponential fit was not extended back to zero onset time but only to peak current time. However, integration was performed back to zero onset time, utilizing pre-peak data points (Fig. 1 *D*). The position of peak current is due to the filtering effects of the clamp amplifier, and, as such, charge should be redistributed in time but not reduced.

RESULTS

OHCs possess a membrane capacitance which depends upon transmembrane voltage. In addition, despite efforts to block nonlinear voltage-dependent conductances, a residual nonlinearity remains. Fig. 2 illustrates the voltage dependence of the membrane capacitance and demonstrates the necessity of correcting for series resistance effects. In this example, a cell was chosen for which the series resistance and membrane resistance were relatively high, 27 and 281 Mohm, respectively (ratio of 0.096). Consequently, the time constants of the capacitive current decay are very large at potentials where the voltage-dependent capacitance is greatest. The series resistance-corrected membrane capacitance (Fig. 2, *solid downward triangles*) is plotted as a function of membrane voltage and fitted (*solid line*) with Eq. 1. The open downward triangles represent apparent capacitance estimates (Q/V_c), i.e., no series resistance corrections were made. Note the large differences in magnitude and voltage dependence between membrane and apparent capacitance. For comparison, the upward triangles represents a model simulation (that of Fig. 1 *A*) utilizing the parameters obtained from the fit to the corrected membrane capacitance data and a linear average membrane resistance. It is clear that the membrane capacitance estimates of the model and the data superimpose, however, apparent capacitance estimates differ somewhat. Finally, the circles illustrate results when the nonlinear leakage conductance found in the biophysical data is included. Again the corrected capacitance data closely corresponds to the biophysical data, but now the apparent capacitance does as well. Simply modeling the cell with only a nonlinear leakage conductance does not generate an artifactual voltage-dependent capacitance. This exercise demonstrates that the method for estimating membrane capacitance (*filled symbols* in Fig. 2) is robust despite the existence of residual nonlinear leakage conductance and indicates that the correction for series resistance is required to obtain accurate estimates of membrane capacitance.

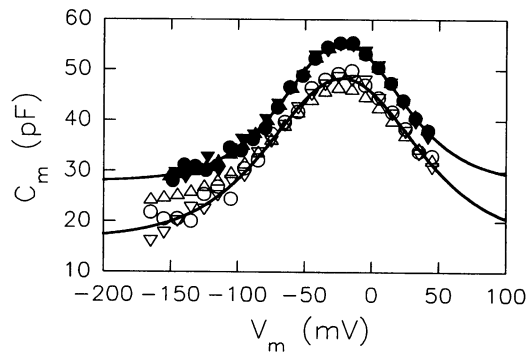

FIGURE 2 voltage-dependent capacitance of guinea pig OHC. Closed symbols indicate the membrane capacitance at each voltage step after correction for series resistance effects. Biophysical data (*downward triangles*), electrical model using fitted parameters of the biophysical data and a linear membrane resistance (*upward triangles*), model incorporating residual nonlinear membrane resistance of the biophysical data (*circles*). The solid line through these data points is a fit with Eq. 1 of the biophysical data (V_h, −27.33 mV; z, 0.829; Q_{max}, 2.66 pC; C_{lin}, 23.24 pF). The open symbols depict the apparent capacitance (Q/V_c) at each step, i.e., no series resistance corrections were made. The solid line through these data points is a fit with Eq. 1 of the biophysical data (V_h, −23.97 mV; z, 0.667; Q_{max}, 3.89 pC; C_{lin}, 14.75 pF). Note the requirement for series resistance correction in order to obtain correct estimates of the membrane capacitance.

An additional 12 cells were recorded from in which the ratio of series resistance to average membrane resistance was fairly low, namely 0.057. Fits to the data indicate that the average maximum nonlinear charge transfer (Q_{max}) is 2.4 pC per cell, with a valence (z) of 0.92. This corresponds to a peak nonlinear capacitance of 21.55 pF at −34.8 mV, riding upon a linear capacitance of 22.7 pF. The linear capacitance corresponds to the estimated whole cell surface area (based on a cylindrical model of the OHC) with the ratio of about 0.01 pF/μm^2 (Fig. 3; however, see Discussion). It should be noted that nonlinear charge movement similar to that representing the motility voltage sensor is not demonstrable in supporting cells and is measurable in OHCs from species other than the guinea pig, e.g., mouse (Fig. 4).

In order to determine whether the motility voltage sensor is distributed within a restricted region of the OHC, a double voltage clamp protocol using two independent clamp amplifiers was employed. That is, utilizing the partitioning microchamber of Evans et al. (1989), in combination with whole cell voltage clamp we are able to electrically amputate that portion of the OHC housed within the chamber (Fig. 5). When identical voltage clamp stimuli are simultaneously delivered to the microchamber and the cell interior, only that portion of the membrane outside the chamber is excited.

The efficiency of this amputation technique is dependent upon the seal (shunt resistance, R_{sh}) which the microchamber makes with the OHC. This is illustrated in Fig. 6, where an

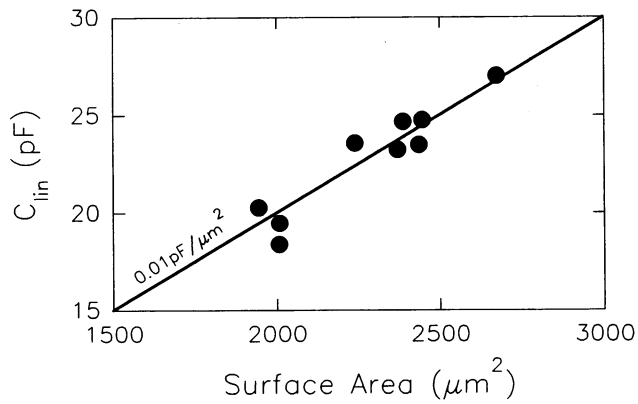

FIGURE 3 Linear capacitance (C_{lin}) versus estimated surface area of OHCs for nine cells.

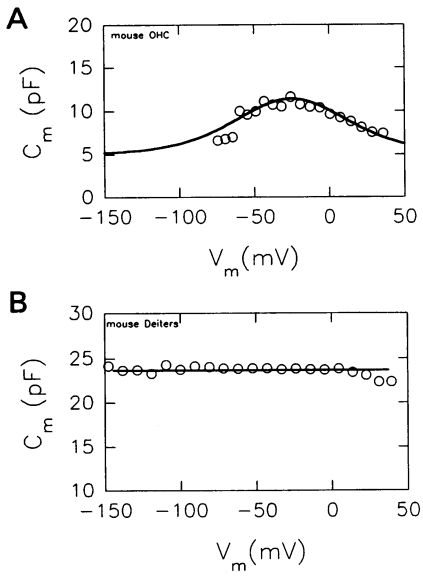

FIGURE 4 (*A*) Nonlinear membrane capacitance of a mouse OHC as a function of membrane potential. Mechanical responses were observed as well. (*B*) Membrane capacitance of a mouse Deiters cell demonstrates no voltage dependence.

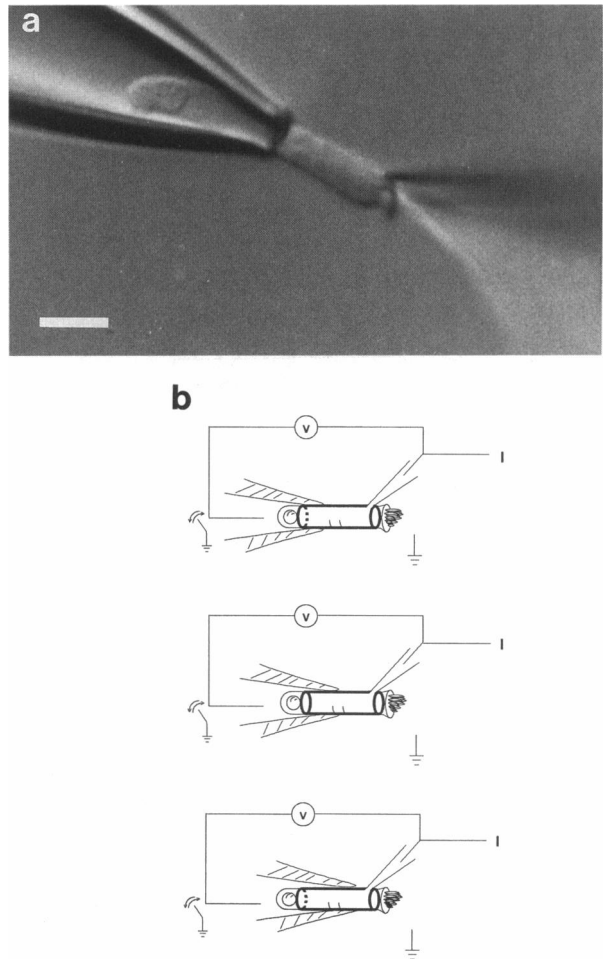

FIGURE 5 (*A*) Photomicrograph of a guinea pig OHC under double voltage clamp condition. Basal region of cell is within microchamber, and whole cell recording is established at the apical region. Scale is 20 μm. (*B*) Diagrammatic representation of the double voltage clamp with the OHC under three different conditions of cell extrusion.

electrical model of the double voltage clamp is evaluated with a model cell partitioned half-way. It is shown that when the shunt resistance is zero (or the chamber voltage is clamped to zero, i.e., ground), the system performs as a simple whole cell voltage clamp, measuring the parallel combination of the internal and external membrane capacitance. A shunt resistance above 5–10 Mohm, which is typical with the technique, provides good estimates of only the external membrane capacitance. By altering the partitioning of an OHC, it is possible to measure changes in linear and nonlinear capacitance utilizing the voltage stair protocol.

Fig. 7 presents the results from an individual OHC for which it was possible to obtain capacitance measures under three partitioning conditions and the whole cell condition. As the cell is extruded from the chamber, both the linear and nonlinear capacitance increase, because increasingly more membrane is exposed to the voltage stimulus (Fig. 7 *A*). Under the assumption that the change in linear capacitance and nonlinear charge (or nonlinear capacitance) is colinear as a function of cell extrusion, that is, that the voltage sensors are evenly distributed within the membrane, a linear fit to the partition data points provides evidence for the existence of a restricted, voltage-sensing region within the OHC (Fig. 7 *B*). The motility data of Dallos et al. (1991) indicates that the motor elements are evenly distributed along the length of the cell. It is likely, therefore, that motility voltage sensors are as well. The linear fit indicates that when the nonlinear charge movement (Q_{max}) reaches zero, linear capacitance is still measurable. That is, as the extent of cell inclusion is increased, a point is reached where nonlinear capacitance is absent, but linear capacitance exists and would continue to decrease with further inclusion. Similarly, as the cell is extruded, Q_{max} reaches a maximum but linear capacitance continues to increase with further extrusion. The slope of the fitted line indicates a charge density of 12,373 e^-/0.01 pF within the voltage-sensing region. As expected, the portion of the cell within the microchamber which experiences no transmembrane voltage drop demonstrates no mechanical response, whereas the portion outside the chamber does (data not shown). However, upon grounding the chamber voltage, mechanical responses of that portion of the cell within the chamber are evident. Thus, the amputation technique also confirms the distributed nature of the mechanical effector (Dallos et al., 1991).

It is extremely difficult to maintain the preparation during changes in partitioning. Nevertheless, it was possible to obtain data on six additional OHCs where at least two partitioning conditions and the whole cell condition were achieved. The average linear capacitance in the apical region of the cells ($n = 7$) where no voltage sensors exist was 4.38 pF. In the base the average was 1.85 pF. The average charge density of the voltage-sensing region for these cells was 10,669 e^-/0.01 pF. The average R_s:R_m ratio for these cells was 0.24.

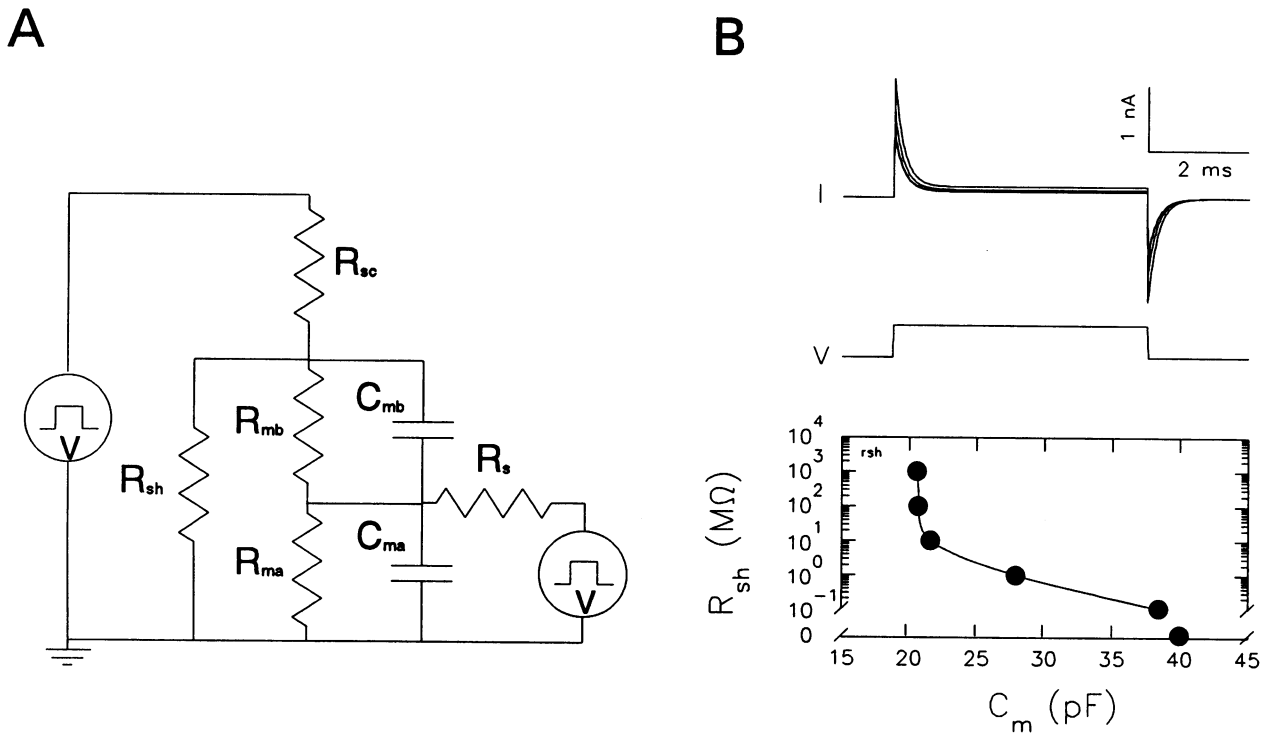

FIGURE 6 (*A*) Electrical model of double voltage clamp. R_{sc}, chamber series resistance; R_s, patch electrode series resistance; R_{sh}, shunt resistance between chamber electrode and ground; R_{mb}, membrane resistance of inserted portion of cell; C_{mb}, membrane capacitance of inserted portion of cell; R_{ma}, membrane resistance of extruded portion of cell; C_{ma}, membrane capacitance of extruded portion of cell. (*B*) The above model was numerically evaluated with parameters representing a cell inserted half way into the chamber, and the shunt resistance was varied to observe the effects on the efficiency of electrical amputation of the inserted portion. R_{sc}, 0.5 MΩ; R_s, 5 MΩ; R_{mb} and R_{ma}, 100 MΩ; C_{mb} and C_{ma}, 20 pF. Current traces (*I*) in response to a 10 mV (*V*) step were used to determine input capacitance (see Methods) as a function of R_{sh}. When R_{sh} is zero the system functions as a simple whole cell voltage clamp, indicating a capacitance of 40 pF. Above 5–10 MΩ, the system provides good indications of that capacitance of the extruded portion of the cell, 20 pF.

DISCUSSION

Several lines of evidence indicate that the mechanical response of the OHC is voltage-dependent (Santos-Sacchi and Dilger, 1988; Iwasa and Kachar, 1989; Ashmore, 1989; Santos-Sacchi, 1991a, 1992). The nonlinear charge movement, which presents itself as a voltage-dependent capacitance, is believed to represent the activity of the OHC's motility voltage sensor. Indeed, many of the characteristics of the nonlinear charge movement correspond to those of the OHC mechanical response, including extent and slope of voltage dependence, kinetics (which have yet to be fully described due to the limitations of the clamp time constant), block by gadolinium ions, and susceptibility to charge screening (Ashmore, 1992; Santos-Sacchi, 1991a, 1992). The present results indicate that the OHC nonlinear capacitance is restricted along the length of the cell, just as the mechanical response is restricted (Dallos et al., 1991).

Estimation of membrane capacitance and nonlinear charge

Under whole cell voltage clamp, OHCs from the apical turn of the cochlea possess a fairly low membrane resistance. Original estimates were between 20 to 40 MΩ (Ashmore and Meech, 1986). More recent average estimates are between 75 and 100 MΩ (Santos-Sacchi and Dilger, 1988; Housley and Ashmore, 1992). Because the ratio of series resistance to membrane resistance under whole cell voltage clamp is not ideal, i.e., zero, it is necessary to correct for series resistance effects. In the present report, membrane capacitance measures were corrected for such effects, and the efficacy of the correction procedure was verified through modeling. Corrections were especially important for those cells partitioned with the microchamber, where the membrane resistance was low (and the R_s:R_m ratio high) as a result of the physical trauma necessarily imposed upon the cell. Eq. 3 indicates that not only corrections to steady state voltage ($V_c \times R_m/R_{in}$) are required, but also corrections to charge magnitude ($Q \times R_{in}/R_m$) are required. In a previous study by Santos-Sacchi (1991), steady state voltage corrections were used to correct voltage dependence measures of nonlinear charge movement; however, corresponding corrections to the charge magnitudes were not made. In that study, average maximum charge movement (2 pC) was probably underestimated. The average Q_{max} in the present study was 2.59 pC ($n = 19$).

Area of OHC devoid of voltage sensors

A linear fit to the partition data points provided average estimates of linear capacitance in the sensor-devoid basal and

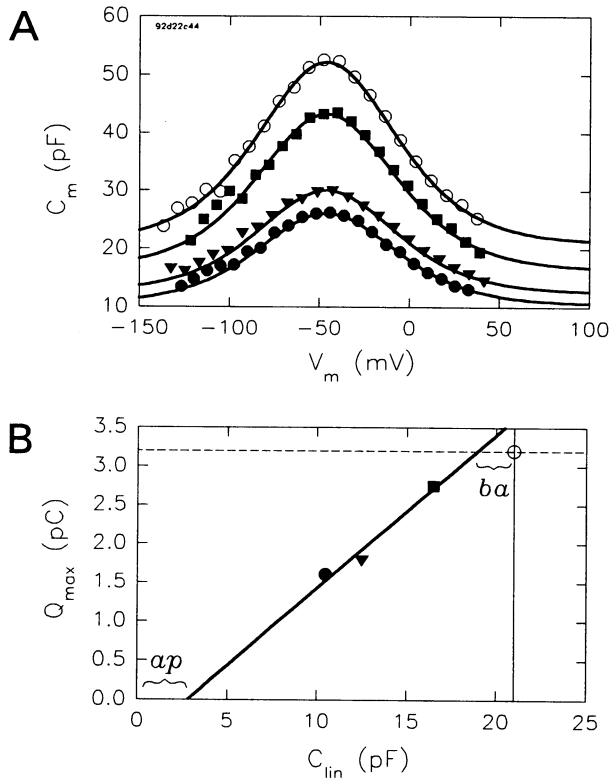

FIGURE 7 (*A*) The voltage-dependent membrane capacitance of a single OHC was evaluated at three levels of partitioning (*closed symbols*) and the whole cell condition (*open symbols*). Linear and nonlinear capacitance decrease as the cell inclusion is increased. The whole cell data were fit using the Nelder-Mead simplex algorithm. Partition data were fit by eye while holding z constant and varying Q_{max}. z: 1. V_h of whole cell data: −46 mV, others shifted to coincide; filled squares, triangles, and circles were −51, −53, and −48 mV, respectively. (*B*) Relation between C_{lin} and Q_{max} determined from above fits for the different levels of partitioning. Linear fit to the partition points indicates the extent of the OHC motility voltage sensor along the length of the cell. The vertical line indicates whole cell linear capacitance; the horizontal dotted line indicates whole cell Q_{max}. Linear capacitance denoted by *ap* (2.65 pF) represents the area of the apical portion of the cell devoid of voltage sensors; that denoted by *ba* (2.06 pF) represents the area of the basal portion of the cell devoid of voltage sensors. Slope of fitted line indicates a charge density of 12,373 e^-/0.01 pF within the sensing region. Ratio of R_s to R_m: 0.19.

apical regions of the OHC. The values were 1.85 and 4.38 pF, respectively. The actual membrane surface area of the OHC is greater than that estimated with light microscopy by a factor of about 1.3 (due to lateral membrane surface crenulation; see Dallos (1983)). This indicates that the linear specific capacitance measures obtained in the present study should be corrected[1] to a value of about 0.008 pF/μm^2. Consequently, the above capacitance values translate to areas of 231 and 547 μm^2, respectively. It is possible to compare these results with the surface areas of OHC plasmalemma which lack adjacent subsurface cisternae and/or mechanical responses.

Microchamber analysis of OHC motility demonstrates that a mechanical response is absent in the cell's most basal region (7 μm in length (B. Evans, personal communication)). The subsurface cisternae are poorly developed or absent in this region, as well. By modeling this basal region of the OHC as a half sphere of 5-μm radius, with a 2-μm cylindrical extension, an area of 220 μm^2 is obtained. This compares favorably with the present estimate of basal surface area lacking voltage sensors. At the apical region of the cell, substantial amounts of subsurface cisternae do not arise until about 5 μm from the top of the cell (Ades and Engstrom, 1974; Saito, 1983). The apical region of the OHC is oddly shaped (Fig. 5 *a*); however, if this portion is modeled as a simple single-ended cylinder (which is likely to underestimate its actual area) with a radius of 5 μm and length of 5 μm, then the calculated surface area is 236 μm^2. Accounting for stereociliar surface area[2] (average of 50 per cell, with a radius of 0.15 μm and length of 6 μm; B. Evans, personal communication), the total apical area increases to 518 μm^2, which is similar to the present estimate of apical surface area lacking voltage sensors. These calculations provide strong support for the notion that the regions of the OHC which lack motility voltage sensors correspond to those which lack subsurface cisternae and/or voltage-dependent mechanical responses. Ultrastructural studies also indicate that only the lateral portion of the OHC plasmalemma possesses dense arrays of intramembranous particles (Saito, 1983; Kalinec et al., 1992).

The correspondence of the nonlinear capacitance with plasmalemmal regions bordering subsurface cisternae may imply some sort of electrical interaction between plasma and subsurface membrane. Such a possibility was considered by Santos-Sacchi (1991a) to account for nonlinear capacitance in this cell. That is, electrical interactions between the two membranous systems might affect capacitance measures, as occurs for input capacitance measures in inner ear supporting cells which are coupled via gap junctions (Santos-Sacchi, 1991b). Recently, however, it has been demonstrated that, following disruption of OHC subsurface structures with intracellularly applied trypsin, mechanical responses of the plasma membrane remain (Kalenic et al., 1992). This indicates that the mechanical effector resides within the plasma membrane. Similar treatments do not abolish the nonlinear capacitance (Huang and Santos-Sacchi, unpublished results), which implies a colocalization of motility voltage sensor and effector within the plane of the plasma membrane. Nevertheless, it is interesting that the subsurface cisternae and voltage sensors coincide, and it is possible that the subsurface

[1]The correction is based on the assumption that the linear-specific capacitance is the same in sensor-containing and sensor-devoid membranes. It is possible that the sensor-containing region has a somewhat higher specific capacitance due to a higher dielectric of the protein particles residing therein. The corrected value should be considered approximate.

[2]While it was often noted that stereociliar were absent in isolated OHCs, it is possible that the isolation procedure caused resorption of the structures. For example, hair cell trauma often causes fusion and clumping of stereocilia (Engstrom, 1983). We never observe isolated stereocilia which may have been sheared off during isolation.

membrane represents a normal molecular turnover route for the motility voltage sensor and/or effector.

Uniform nature of voltage sensors within the OHC

It has previously been noted that some of the nonlinear charge movement in OHCs should be due to gating of voltage-dependent ionic channels (Santos-Sacchi, 1991a). However, while the supporting cells undoubtedly possess channel gating charge, charge movement of the magnitude recorded in OHCs is not seen. It appears that the charge moved by the motility voltage sensor far outweighs that contributed by channel gating, indicating that the characteristics of the nonlinear charge movement in the OHC overwhelmingly reflect that of the motility mechanism. Using similar logic, Fernandez et al. (1983) were able to evaluate characteristics of the membrane bound charge movement produced by the lipophilic molecule DpA^- despite the existence of smaller channel gating charge.

Some aspects of the nature of the voltage sensors along the length of the OHC can be gleaned from the results of the partitioning experiments. That is, it is possible to determine whether sensor characteristics (e.g., voltage sensitivity) along the extent of the active, voltage-sensing region vary from the average obtained under whole cell conditions. The only factor which changed significantly during changes in the degree of partitioning was the value of Q_{max} (except for the linear capacitance, of course). That is, the same nonlinear capacitance function (namely, z kept constant) which fit the whole cell data could adequately describe capacitance measures obtained from increasingly smaller portions of the cell. V_h was seen to vary sometimes, and may be due to charge screening effects, or changes in the metabolic state of cells during the course of the experiments. For example, it is known that phosphorylating agents can shift V_h without altering other parameters of the OHC nonlinear capacitance function (Huang and Santos-Sacchi, 1993). The maintenance of the form of the C_v function during successive amputations indicates that the nature of the voltage sensor along the extent of the OHC is constant, and that partitioning simply alters the number of sensors which are activated. That is, the voltage sensors (and possibly effectors) are probably of one type along their extent.

Density of voltage sensors

The number of independent elementary charges moved per square micrometer has previously been estimated to be about 4000 (Santos-Sacchi, 1991a), based on a Q_{max} of 2 pC and a total surface area of a model OHC of 70-μm length. In the present report, the linear capacitance values obtained in whole cell configuration translate to an average membrane surface area of 2917 μm^2 (n = 19). Thus, with the present Q_{max} value of 2.59 pC, an average charge density of 5542 e^-/um^2 is obtained. However, it is now clear that the extent of the OHC motility voltage sensors is restricted along the length of the cell. It is necessary, therefore, to compute charge density based on surface area estimates for that portion of the OHC which possesses the motility voltage sensors. After removing the average surface area of the OHC devoid of voltage sensors (sum of apex and base: 6.23 pF or 778 μm^2 (n = 7)) from the total average surface area, we obtain an average charge density of 7558 $e^-/\mu m^2$. Since the voltage dependence of the nonlinear charge movement and motility are comparable (z close to 1 (Ashmore, 1992; Santos-Sacchi, 1991a)), it is concluded, based on a two-state model, that about 7500 $e^-/\mu m^2$ independent elementary charged particles control the mechanical activity of the OHC. It is tempting to attribute the measured charge movement to integral membrane proteins represented by the membrane particles observed in the lateral plasmalemma of the OHC (Gulley and Reese, 1977; Saito, 1983; Forge, 1991; Kalinec et al., 1992). In a similar fashion, Roberts et al., (1990) suggested, based on colocalizing ultrastructural and electrophysiological evidence, that membrane particles located at synaptic areas of the hair cell may represent K^+ and Ca^{2+} channels. One possible interpretation of the colocalization of sensor and effector along the length of the OHC is that the sensor and effector reside within one molecular species, similar to ionic channels where sensor movement in an electrical field is believed to promote gating via a conformational change of the channel protein.

However, the present charge density estimate is no longer in line with the suggestion of Santos-Sacchi (1991a) that the number of elementary charges corresponds to the number of particles observed ultrastructurally in the OHC lateral membrane. Recent estimates of the number of membrane particles indicate about 2500/μm^2 (Holley et al., 1992). It may be that each membrane particle possesses three charges which must each independently move between two states to effect a mechanical response. An interesting reinterpretation of the OHC charge data may be made by utilizing the electrodiffusion model of Neumcke et al. (1978), in which charge movement is viewed as a multistate phenomenon. For example, using this Langevin type fit to their data, they determined that the valence (z) of Na^+ channel nonlinear charge movement was about three times that of a two-state model. The multistate model more accurately accounted for Na^+ channel gating and conductance characteristics. Drews (1988) reached a similar conclusion. Under such an interpretation, the valance (z) of OHC charge movement would be closer to 3, and this might suggest that three charges correspond to each ultrastructurally observed membrane particle, all charges needing to traverse a characteristic distance across the membrane before a mechanical effect ensues. The multistate model would predict that the onset of the mechanical response would be delayed following a step voltage stimulus, and this type of response has been observed (Ashmore, 1987; Santos-Sacchi, 1992). However, because of the limitations of clamp amplifier speed, the true time course of the OHC mechanical response is not known (Santos-Sacchi, 1992). In addition, a loss of OHC cell turgor (known to interfere with OHC motility (Holley and Ashmore, 1988;

Santos-Sacchi, 1991a)) which necessarily accompanies whole cell voltage clamp configuration, may also contribute to a delayed response. It cannot be judged at this point whether charge movement in the OHC is two-state or multistate.

APPENDIX

For the model (Fig. 1 *A*), the steady state (I_∞) and instantaneous (I_0) current responses to a voltage step are defined as

$$I_\infty = \frac{V_c}{R_s + R_m}, I_0 = \frac{V_c}{R_s}. \quad (6)$$

with the exponentially decaying capacitive current given as

$$I_{C_m} = (I_0 - I_\infty)e^{\frac{-t}{\tau}}, \quad (7)$$

where

$$\tau = R_\parallel C_m, \quad (8)$$

$$R_\parallel = \frac{R_m R_s}{R_{in}}, \quad (9)$$

and

$$R_{in} = R_m + R_s, \quad (10)$$

the input resistance readily obtained at steady state.

The charge moved is then obtained by integration

$$\int_0^\infty I_{C_m} dt = Q = \frac{C_m R_m^2 V_c}{R_{in}^2}. \quad (11)$$

Solving for C_m,

$$C_m = \frac{R_{in}^2 Q}{R_m^2 V_c}, \quad (12)$$

and utilizing Eqs. 4 and 8, we obtain

$$R_s = \frac{R_{in}\tau V_c}{QR_{in} + \tau V_c}. \quad (13)$$

The time constant (τ) of the exponentially decaying current, and the charge moved (Q) are little affected by filter settings as low as 2 kHz (eight-pole Bessel).

We thank Frank N. Tilley III for technical assistance. Thanks also to Dr. H. Sontheimer for comments on the manuscript, and Drs. F. Bezanilla and K. Chandler for many helpful discussions.

This work was supported by National Institutes of Health-National Institute of Deafness and other Communication Disorders grant DC00273.

REFERENCES

Ades, H. W., and H. Engstrom. 1974. Anatomy of the inner ear. *In* Handbook of Sensory Physiology, Vol. V/1. W. D. Keidel and W. D. Neff, editors. 125–158.

Ashmore, J. F. 1987. A fast motile response in guinea-pig outer hair cells: the cellular basis of the cochlear amplifier. *J. Physiol. (Lond.).* 388: 323–347.

Ashmore, J. F. 1989. Transducer motor coupling in cochlear outer hair cells. *In* Mechanics of Hearing. D. Kemp and J. P. Wilson, editors. Plenum Press, New York. 107–113.

Ashmore, J. F. 1992. Mammalian hearing and the cellular mechanisms of the cochlear amplifier. *In* Sensory Transduction. D. P. Corey, and S. D. Roper, editors. Rockefeller University Press, New York, p. 395–412.

Ashmore, J. F., and R. W. Meech. 1986. Ionic basis of the resting potential in outer hair cells isolated from the guinea pig cochlea. *Nature.* 322: 368–371.

Brownell, W. E., C. R. Bader, D. Bertrand, and Y. de Ribaupierre. 1985. Evoked mechanical responses of isolated cochlear outer hair cells. *Science (Wash. DC).* 227:194–196.

Dallos, P., J. Santos-Sacchi, and Å. Flock. 1982. Intracellular recordings from outer hair cells. *Science (Wash. DC).* 218:582–584.

Dallos, P. 1983. Some electrical circuit properties of the organ of Corti. I. Analysis without reactive elements. *Hear. Res.* 12:89–119.

Dallos P, B. N. Evans, and R. Hallworth. 1991. On the nature of the motor element in cochlear outer hair cells. *Nature (Lond.).* 350:155–157.

Drews, G. 1988. Effects of aconitine and batrachotoxin on Na currents and gating currents in the frog node of Ranvier. *Pflugers Arch. Eur J. Physiol.* 411:491–499.

Engstrom, B. 1983. Stereocilia of sensory cells in normal and hearing impaired ears. *Scand. Audiol. Suppl.* 19:1–34.

Evans, B. N., P. Dallos, and R. Hallworth. 1989. Asymmetries in motile responses of outer hair cells in simulated in vivo conditions *In* Mechanics of Hearing. D. Kemp, and J. P. Wilson, editors. Plenum Press, New York. 205–206.

Fernandez, J. M., R. E. Taylor, and F. Bezanilla. 1983. Induced capacitance in the squid giant axon. Lipophilic ion displacement currents. *J. Gen. Physiol.* 82:331–346.

Forge, A. 1991. Structural features of the lateral walls in mammalian cochlear outer hair cells. *Cell Tissue Res.* 265:473- 483.

Gulley, R. L., and T. S. Reese. 1977. Regional specialization of the hair cell plasmalemma in the organ of Corti. *Anat. Rec.* 189:109–124.

Holley, M. C., and J. F. Ashmore. 1988. On the mechanism of a high-frequency force generator in outer hair cells isolated from the guinea pig cochlea. *Proc. R. Soc. Lond. Ser. B Biol. Sci.* 232: 413–429.

Holley, M. C., F. Kalenic, and B. Kachar. 1992. Structure of the cortical cytoskeleton in mammalian outer hair cells. *J. Cell Sci.* 102:569–580.

Housley, G. D., and J. F. Ashmore. 1992. Ionic currents of outer hair cells isolated from the guinea-pig cochlea. *J. Physiol. (Lond.).* 448:73–98.

Huang, G., and J. Santos-Sacchi. 1993. Metabolic control of OHC function: phosphorylation and dephosphorylation agents shift the voltage dependency of motility related capacitance. Proceedings of Midwinter Meeting of the Association for Research in Otolaryngology, St. Petersburg, FL, February.

Iwasa, K. H., and B. Kachar. 1989. Fast in vitro movement of outer hair cells in an external electric field: effect of digitonin, a membrane permeabilizing agent. *Hear. Res.* 40:247–254.

Kalinec, F., M. C. Holley, K. H. Iwasa, D. J. Lim, and B. Kachar. 1992. A membrane-based force generation mechanism in auditory sensory cells. *Proc. Natl. Acad. Sci. USA.* 89:8671–8675.

Mathias, R. T., R. A. Levis, and R. S. Eisenberg. 1981. An alternative interpretation of charge movement in muscle. *In* The Regulation of Muscle Contraction: Excitation-Contraction Coupling. A. D. Grinnell and M. A. B. Brazier, editors. Academic Press, New York. 39–52.

Neumcke B, W. Nonner, and R. Stampfli. 1978. Gating currents in excitable membranes. International Review of Biochemistry, 19, 129–155.

Roberts, W. M., R. A. Jacobs, and A. J. Hudspeth. 1990. Colocalization of ion channels involved in frequency selectivity and synaptic transmission at presynaptic active zones of hair cells. *J. Neurosci.* 10:3664–3684.

Ruggero, M. A. 1992. Responses to sound of the basilar membrane of the mammalian cochlea. *Current Opinion in Neurobiology* 2:449–456.

Saito, K. 1983. Fine structure of the sensory epithelium of guinea pig organ of Corti: subsurface cisternae and lamellar bodies in the outer hair cells. *Cell Tissue Res.* 229:467–481.

Santos-Sacchi, J. 1990. Fast outer hair cell motility: how fast is fast? *In* The

Mechanics and Biophysics of Hearing. P. Dallos, C. D. Geisler, J. W. Matthews, M. A. Ruggero, C. R. Steele, editors. Springer-Verlag, Berlin. 69–75.

Santos-Sacchi, J. 1991a. Reversible inhibition of voltage-dependent outer hair cell motility and capacitance. *J. Neurosci.* 11:3096–3110.

Santos-Sacchi, J. 1991b. Isolated supporting cells from the organ of Corti: some whole cell electrical characteristics and estimates of gap junctional conductance. *Hear. Res.* 52:89–98.

Santos-Sacchi, J. 1992. On the frequency limit and phase of outer hair cell motility: effects of the membrane filter. *J. Neurosci.* 12:1906–1916.

Santos-Sacchi, J. 1993. Voltage-dependent ionic conductances of Type I spiral ganglion cells from the guinea pig inner ear. *J. Neurosci.* 13:3599–3611.

Santos-Sacchi, J., and J. P. Dilger. 1988. Whole cell currents and mechanical responses of isolated outer hair cells. *Hear. Res.* 35:143–150.

Santos-Sacchi, J. and Huang, G.-J. 1993. Characterizing the extent of the OHC motility voltage sensor with an electrical guillotine: evidence that ends don't meet. Symposium on the Biophysics of hair cell sensory systems. Paterswolde, The Netherlands, June.